Electronic Supplementary Material (ESI) for Chemical Communications.
This journal is © The Royal Society of Chemistry 2019

SUPPORTING INFORMATION

An aminoglycoside antibiotic inhibits both lipid-induced and solution-phase fibrillation of α-Synuclein *in vitro*

Anindita Mahapatra[a,b], Sukanya Sarkar[c], Subhash Chandra Biswas[c] and Krishnananda Chattopadhyay[a,b*]

Corresponding author email: krish@iicb.res.in

a. Structural Biology and Bio-informatics Division, Indian Institute of Chemical Biology, Kolkata-700032, India

b. Academy of Scientific and Innovative Research (AcSIR), Ghaziabad- 201002, India

c. Cell Biology and Physiology Division, Indian Institute of Chemical Biology, Kolkata-700032, India

Table of Contents [TOC]:

1. MATERIALS AND METHODS

1.1. Protein purification of A-Syn. For the expression and purification of A-Syn, we purchased isopropyl β-D-galactopyranoside (IPTG) and Tris salt from Biotecx Laboratories (Houston, TX) and J.T. Baker (Center Valley, PA), respectively. Phenylmethanesulfonylfluoride (PMSF), ammonium sulfate, and sodium chloride were obtained from Sigma-Aldrich (St. Louis, MO). Recombinant human A-Syn was expressed in Escherichia coli BL21 (DE3) strain transformed with pRK172 α-Synuclein WT plasmid. The expression was induced using 1 M IPTG at an OD of 0.5−0.6. The cultures were incubated at 37 °C with shaking at 175 rpm for 4 h after addition of IPTG. Cells were then harvested by centrifugation. The cell pellets were then resuspended in sonication buffer (10 mM Tris, pH = 7.4) and lysed by sonication using short but continuous pulses at 12 Hz for 1 min. This step was repeated 14 times to lyse all the cells. The lysate was centrifuged at 14000 rpm for 45 min at 4 °C to remove cell debris. Just before the sonication, 1 mM PMSF cocktail was added. The lysis suspension was brought to 30% saturation with ammonium sulfate and the pellet was discarded. It was followed by 50% saturation with ammonium sulfate. The solution was then centrifuged at 35000 rpm for 1 h at 4 °C. The resultant pellet was dissolved in 20 mM Tris buffer, pH 7.4 and dialyzed overnight against same buffer. After dialysis, the protein sample was filtered using 30 kDa centricon filter. The crude protein was then injected into a DEAE anion exchange column equilibrated with 10 mM Tris (pH = 7.4) and eluted using a NaCl gradient. A-Syn was found to elute at about 300 mM NaCl. Fractions containing A-Syn (analyzed by Coomassie-stained SDS-PAGE) were concentrated and further purified using a Sephadex gel filtration column. Fractions containing A-Syn were combined and lyophilized. For the sample preparation of all experiments, lyophilized protein was dissolved in NaP buffer (20 mM Sodium phosphate, pH 7.4) and filtered using 0.22 μm low protein binding membranes (Millex-GP). This was followed by centrifugation at 15,000 g for 1 hr at 4 ^{0}C for removal of traces of small oligomeric forms of the protein that may form during purification and storage.[1] This step is essential because the presence of small amount of oligomers can act as seeds for further fibrillation.

1.2. Preparation of vesicles. DOPS and DOPE/DOPS/DOPC mixture with a 5:3:2 weight ratio (Coagulation Reagent I) were purchased from Avanti Polar Lipids as lyophilized powder. Vesicles were prepared by sonication method as described previously[2] in NaP buffer. Briefly, required weight of lyophilized powder (for 2.5 or 5 mM solution) was suspended in NaP buffer and the mixture vortexed for 10 minutes. This was followed by 30 minutes of sonication in Qsonica sonicator of model number Q500 (amplitude 35 %, on-pulse of 30 s and off-pulse of 45 s).

For preparing Laurdan-loaded vesicles, the required amounts of chloroform stocks of the lipid (DOPS/Coagulation Reagent I) and dye, calculated to obtain a final concentration of 2.5 mM for the lipids and 25 μM for the probe, were mixed in glass vials. The chloroform solvent was first evaporated under nitrogen flow and then under vacuum for 2 hours. Then required amount of buffer was added and SUVs prepared as usual.

For preparing Calcein-loaded mimic SUVs, lyophilised lipid mixture composed of 30% 1,2-dioleoyl-sn-glycero-3-phospho-L-serine (DOPS), 50% 1,2-dioleoyl-sn-glycero-3phosphoethanolamine (DOPE), and 20% 1,2-dioleoyl-sn-glycero-3phosphocholine (DOPC) was suspended in 500 μL of 70 mM Calcein in NaP buffer, at a final lipid concentration of 1 mg/mL. The suspension was vortexed for 10 minutes followed by sonication, to prepare SUVs as usual. The formation of SUVs was checked by Dynamic Light Scattering, followed by separation of Calcein- loaded SUV from free dye using PD-10 desalting column (GE Healthcare).[3]All prepared SUVs were stored at 4°C for future use.

1.3. Dynamic Light Scattering (DLS) and Zeta (ζ) Potential Measurements. The ζ-potential and size distribution experiments were conducted with a lipid concentration of 50 μM at 25 °C using the Nano-ZS instrument (Malvern Instruments, Worcestershire, U.K.) at 25 °C (5 mW, He−Ne laser, λ = 632 nm, scattering angle = 173°). For determining size distributions by DLS, the operation procedure was programmed using the DTS software supplied with the instrument to record the average of an automated number of runs. Every run was collected for 10 s, and an equilibration time of 5 min was used, prior to starting the measurement. Characterization of the different types of lipid vesicles by this method showed that the main population of vesicles (by number) had hydrodynamic diameters around 20-25 nm for all except Calcein loaded ones that were ~ 80 nm in diameter. (Fig. S3A, Fig. S21). DLS was used to study the effect (if any) of Kanamycin on model and mimic SUVs, for which size distributions were recorded for the lipid solution alone, followed by addition of increasing amounts of Kanamycin, for each of the two types of lipid used. Moreover, the change in particle size during aggregation of A-Syn with and without Kanamycin was recorded using DLS.

Screening of negative charges on SUV surface by Kanamycin was observed from zeta potential measurements of vesicles with and without increasing concentrations of the antibiotic added. Samples for ζ-potential measurements were loaded into a folded capillary cell and average zeta potential values obtained from an automated number of runs (maximum 100) were noted. The instrument measured ζ-potential from the electrophoretic mobility (μ), using a model described by the Smoluchowski equation.

1.4. Thioflavin T (ThT) binding assay. For monitoring lipid-induced pathway, 500 μL of 5 μM protein in NaP buffer was incubated with each of 50 μM model and mimic SUVs, in presence of 1 mM sodium azide (to prevent bacterial contamination), and increasing concentrations of KMS, under shaking conditions at 180 rpm at 37 °C. KMS concentrations were varied from a ratio of 1:1 to 1:30 w.r.t protein. In case of solution-phase fibrillation, effect of KMS on primary nucleation was studied by incubating 100 μM of A-Syn in PBS (Phosphate Buffered Saline) separately with and without increasing concentrations of KMS (10, 100 and 1000 μM), under shaking conditions at 180 rpm and 37 °C. For studying the effect of KMS on secondary nucleation of A-Syn, pre-formed fibrils (PFFs) were formed by agitation-incubation of monomeric A-Syn for ~96 hours, collected by centrifugation, re-suspended in PBS and sonicated to generate fibril seeds. 1 mol% of the resultant seeds was added to fresh 100 μM monomeric A-Syn, either with or without different doses of added KMS (10, 100 and 1000 μM) and incubated as before. In order to study effect of KMS on PFFs, PFFs were made by agitation-incubation of monomeric A-Syn in PBS for ~96 hours, collected by centrifugation and re-suspended in PBS, followed by incubation with or without increasing doses of KMS. In each case, suitable aliquots were withdrawn at different time-points of the aggregation pathway and diluted in NaP buffer to a total volume of 500 μL, keeping the working concentration of protein at 2 μM and a protein:ThT ratio of 1:10 for the lipid-induced pathway and 1:2 for the solution-phase one. The steady state fluorescence of ThT was measured with proper mixing in a quartz cuvette of 1 cm path length, using excitation at 440 nm and emission at 485 nm. Fluorescence measurements were carried out using a PTI fluorimeter, using excitation and emission slit widths at 5 nm, integration time of 0.1 s, and averaging over 3 measurements. Fibrillation kinetics data (of A-Syn systems that gave a sigmoidal profile) were fit into the Boltzmann equation (Eq. 1) as follows:

$$y = y_0 + \frac{A}{1+\exp(k'(t-t_{0.5}))} \quad (1)$$

where y_0 is the signal base line at the beginning, A is the total increase in fluorescence signal, k´ is the growth rate constant and $t_{0.5}$ is the mid-point of the transition. From $t_{0.5}$ the lag time is calculated by the following equation:

$$t_{lag} = t_{0.5} - 1/2k' \quad (2)$$

where t_{lag} is defined as the time point where amplitude of the transition is 10% of the whole transition.

1.5. Atomic Force Microscopy. For AFM imaging, 5 μL sample was deposited on a freshly cleaved muscovite ruby mica sheet (ASTM V1 grade ruby mica from MICAFAB, Chennai) followed by

incubation in room temperature for 10 minutes. The dried sample was then gently washed with 100 µL of Milli-Q water to remove salt and loosely bound protein moieties. Acoustic alternate current (AAC) mode AFM was performed using a Pico Plus 5500 AFM (Agilent Technologies, USA) with a piezoscanner having a maximum range of 9 µm. Microfabricated silicon cantilevers of 225 µm in length with a nominal spring force constant of 21−98 N/m were obtained from Nano Sensors. The cantilever oscillation frequency was tuned to the resonance frequency. The cantilever resonance frequency was 150−300 kHz. The images (256 pixels × 256 pixels) were captured with a scan size of between 0.5 and 5 µm at a scan speed of 0.5 lines/s. Images were processed by flattening using PicoView software (Agilent Technologies, USA). The length, height, and width of protein aggregates were measured manually using PicoView software.

1.6. Binding and Phase-shift assay using Steady State Fluorescence Spectroscopy. A steady state fluorescence spectroscopic assay has been used for studying the binding of A-Syn to model and mimic SUVs in the absence and presence of KMS. For sample preparation, initially a required volume of 100 µM SUVs in NaP buffer, was incubated overnight at 37 °C, with 0.5 wt % of membrane-specific DiI C-18 dye.[4] This dye is a lipophilic carbocyanine that is weakly fluorescent in water but highly fluorescent and quite photostable when incorporated into membranes. Once added to membranes they diffuse laterally into them and become fluorescent in the hydrophobic environment.[5] Such sensitivity of these dyes to their surrounding environment makes them excellent candidates to monitor protein-lipid (vesicle) binding. A binding that causes the dye to be incorporated further inside the hydrophobic interiors of the lipid bilayer, would lead to enhanced fluorescence. On the other hand, binding interaction that causes translocation of dye molecules to the water-exposed membrane exteriors or their expulsion from lipid surface should show reduced fluorescence from the dye. Alternatively, the hydration dynamic at the membrane−solvent interface may get altered due to the lipid−protein interaction modulating the relaxation behavior and hence fluorescence intensity of DiD.Binding of protein was studied by titrating A-Syn into 50 µM of dye-incorporated lipid (model/mimic), with or without prior addition of 50 µM KMS. In all cases, the steady-state fluorescence emission spectra of the dye were recorded at an excitation wavelength of 600 nm. The peak (fluorescence) intensity values at 675 nm (for model) and 680 nm (for mimic) were plotted against protein concentration and were fit using the Hill Equation (Eq. 3) given by:

$$F = F_0 + \frac{(F_e - F_0)x^n}{x^n + K^n} \quad (3)$$

with F and F_0 referring to the fluorescence intensity of DiI C-18 in the presence and absence of protein, respectively. F_e denotes the minimum/maximum intensity in the presence of a higher

concentration of protein, and K is the equilibrium dissociation constant of the lipid−protein complex. 'n' is the Hill coefficient, which measures the cooperativity of binding, and x is the concentration of the protein.

For studying the effect of KMS on the phase composition of the lipids used, 50 μM of Laurdan-loaded SUVs were titrated by increasing amounts the antibiotic. Laurdan is a lipid-staining dye that shows characteristically different emission depending on the ordering of the membrane bilayer.[6,7] For a given excitation wavelength (usually 340 nm), emission intensities at 490 and 440 nm correspond to contributions from the fluid and gel phases respectively, so that a ratio of the two can be used as a measure of the relative content of fluid and gel phases in the lipid. Hence the samples were excited at 340 nm and the ratio of the emission intensity values at 490 and 440 nm (characteristic of the liquid crystalline and gel phases respectively) were plotted against concentrations of titrant to observe the extent of phase shift caused by KMS to each of the two types of lipids.

1.7. Circular Dichroism. To see how KMS interfered with binding of protein to the two different types of lipid, a volume of 400 μL of 5 μM A-Syn in NaP buffer was treated with 50 μM of each type of vesicle (~20-25 nm diameter), and the same with increasing amounts of Kanamycin monosulfate (KMS) solution added to it, in the ratio ranging from 1:10 to and 1:100 w.r.t protein. The CD spectrum of only 5 μM protein with 100 times KMS was also recorded for comparison. The secondary structure change of each sample was monitored using a JASCO J815 CD instrument. Other parameters included scan speed of 100 nm/ min, integration time of 1 s, and number of acquisitions equal to 3. CD measurements were carried out between 195 and 250 nm using the permissible HT voltage to obtain optimum signal-to-noise ratio. A traditional CD cuvette of 0.1 cm path length was used for the far UV CD measurements. The fraction of lipid bound A-Syn was calculated as per earlier reports[8] using Eq. 4 as follows:

$$x_{bound} = \frac{Ellipticity_{mes} - Ellipticity_{free}}{Ellipticity_{bound} - Ellipticity_{free}} \quad (4)$$

With $Ellipticity_{mes}$, $Ellipticity_{free}$ and $Ellipticity_{bound}$, being the values of Ellipticity measured at 222 nm for a given concentration of KMS, that of free monomeric A-Syn and that of A-Syn with 10 times lipid respectively.

In order to monitor conformational change during aggregation pathway of A-Syn with and without Kanamycin, CD spectra were recorded at different time points of aggregation, when aliquots from the aggregation samples were diluted into a volume of 400 μL to achieve a final concentration of 5

μM just before recording. Difference spectra were obtained by subtracting one spectrum from another, and the peaks observed therefrom were assigned in accordance with an earlier report on accurate secondary structure prediction by CD.[9]

1.8. Fourier Transform Infrared (FTIR) Spectroscopy. FTIR spectra of 100 μM A-Syn, 100 uM A-Syn with each of 1000 μM model and mimic SUVs and the same with 1000 μM KMS added, were recorded using a Bruker 600 series FT-IR spectrometer, in the ATR (Attenuated Total Reflection) mode. The deconvolution of background-corrected baseline-subtracted spectra in the amide I region (from 1700 to 1600 cm−1) was done by least-squares iterative curve fitting to Gaussian/ Lorentzian line shapes. The assignment of peaks was done using previously described spectral components associated with different secondary structures, which vary slightly from one report to another.[10-13] In general, bands in the range of 1611−1630 cm^{-1} are attributed to cross-β, those in the range of 1630−1637 cm^{-1} to parallel β-sheet/extended strands, those in the range of 1637- 1649 cm^{-1} to disordered, those in the range of 1649−1662 cm^{-1} to α-helix, those in the range of 1662−1682 and 1690− 1695 cm^{-1} to loops and turns, and those in the range of 1682−1689 cm^{-1} to antiparallel β-sheet.

1.9. Calcein release assay. 10 μM Calcein loaded lipid vesicles were incubated overnight with 10μM pre-formed aggregates formed with and without added KMS (1:1 and 1:10 w.r.t. protein), and monitored for Calcein release. The fluorescent intensity of the different mixtures were monitored at λ_{exc} = 490 nm, λ_{em} = 510 nm in a PTI fluorimeter. Total dye release was completed by the addition of 0.1 vol % Triton X-100.[3] The percentage of probe release was calculated as follows:

$$\% \text{ Dye release} = (IF-IB)/(IT-IB) \times 100 \quad (5)$$

where IF, IT, and IB are the fluorescence intensity of the dye released by the protein, total dye released, and control blank. Statistical data analysis was performed using one-way ANOVA analysis (Tukey's post-hoc) in the GraphPad Prism 6 software, where ns: non-significant, *: $p \leq 0.05$, **: $p \leq 0.01$, ***: $p \leq 0.001$, ****: $p \leq 0.0001$.

1.10. SHSY5Y cell culture. SHSY5Y is a human-derived cell line sub-cloned from the original cell line named SK-N-SH earlier acquired from bone marrow biopsy of a four-year old female with neuroblastoma. It is often used as an *in vitro* model for neuronal function and differentiation. It was maintained in Dulbecco's Modified Eagle Medium (DMEM) supplemented with 10% fetal bovine serum (FBS) and 1% penicillin/streptomycin (PS), at 37 °C and 5% CO_2, with passage at confluency. For differentiation into neuron like cells the media was changed with 10μM of all-trans retinoic acid

added to DMEM with 1% FBS every alternate day for 7-8 days till extended neuronal processes were observed. MTT reduction assay was performed with undifferentiated SHSY5Y while Flow Cytometry was done with the differentiated cells.

1.11 Cell viability assay. Cell viability assays were performed using the principle of reduction of 3-(4,5-dimethylthiazol-2-yl)-2,5-diphenyl tetrazolium bromide (MTT) by viable cells. For this, cells were seeded in 96-well plates at 30,000 cells/well, and maintained in 200 µl of DMEM supplemented with 10% FBS and 1% PS for 24 h at 37 °C. Aggregates of 48 hour and 96 hour time-points formed in the absence and presence of 10 times KMS, were added to the cell culture medium. Also, PFFs incubated alone and with 10 times KMS for 1 h at 37 °C under shaking conditions, were added as separate treatments. Control treatment containing only 100 µM KMS was also kept. After treatment, cells were incubated for 24 h at 37 °C and 5% CO_2, following which the MTT reduction assay was performed as previously described.[14] All experiments were performed in quadruplicate, and the relative cell viability (%) was expressed as a percentage relative to the untreated cell control. Statistical data analysis was performed using one-way ANOVA analysis (Tukey's post-hoc) in the GraphPad Prism 6 software, where ns: non-significant, *: $p \leq 0.05$, **: $p \leq 0.01$, ***: $p \leq 0.001$, ****: $p \leq 0.0001$.

1.12. Flow Cytometry. For the flow cytometric determination of the percentage of apoptotic/necrotic cells using Annexin V/Propidium Iodide (PI) staining, SHSY5Y cells were seeded in 6-well plates at 3 lac cells/well, followed by treatment for differentiation to neurons (secondary) as described before. Then aggregates of 48 hour and 96 hour time-points formed in the absence and presence of 10 times KMS, were added to the cell culture medium. Also, PFFs incubated alone and with 10 times KMS for 1 h at 37 °C under shaking conditions, were added as separate treatments. Control treatment containing only 100 µM KMS was also kept. After treatment, cells were incubated for 24 h at 37 °C and 5% CO_2, following which the percentage of necrotic cells were determined using the Dead Cell Apoptosis Kit by Invitrogen, following instructions from the manufacturer. The BD LSRFortessa (Flow Cytometer) was used for the Fluorescence Activated Cell Sorting (FACS) of apoptotic, necrotic and viable cell populations. Necrosis is believed to be an important pathway of cell death in PD pathology.[15,16] Among other things, necrotic cell death is characterised by cell membrane rupture and dilation of nuclear membrane to release nuclear materials. Thus the nucleic acid binding dye PI can stain necrotic cells by binding to exposed nuclear materials, and gives red fluorescence that can be detected by the Flow Cytometer, and processed to give the percentage of necrotic cells in any given sample. Statistical data analysis was performed using one-way ANOVA

analysis (Tukey's post-hoc) in the GraphPad Prism 6 software, where ns: non-significant, *: $p \leq 0.05$, **: $p \leq 0.01$, ***: $p \leq 0.001$, ****: $p \leq 0.0001$.

2. SUPPLEMENTARY FIGURES AND TABLES

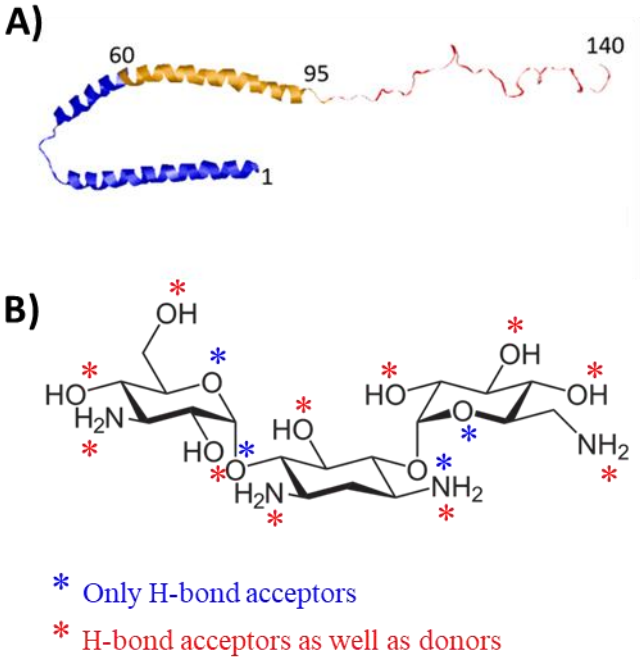

Figure S1. A) Structure of lipid-bound alpha synuclein from Protein Data Bank (PDB Id: 1XQ8), visualized and colored using Rasmol. B) Structure of Kanamycin, showing H-bonding functionalities.

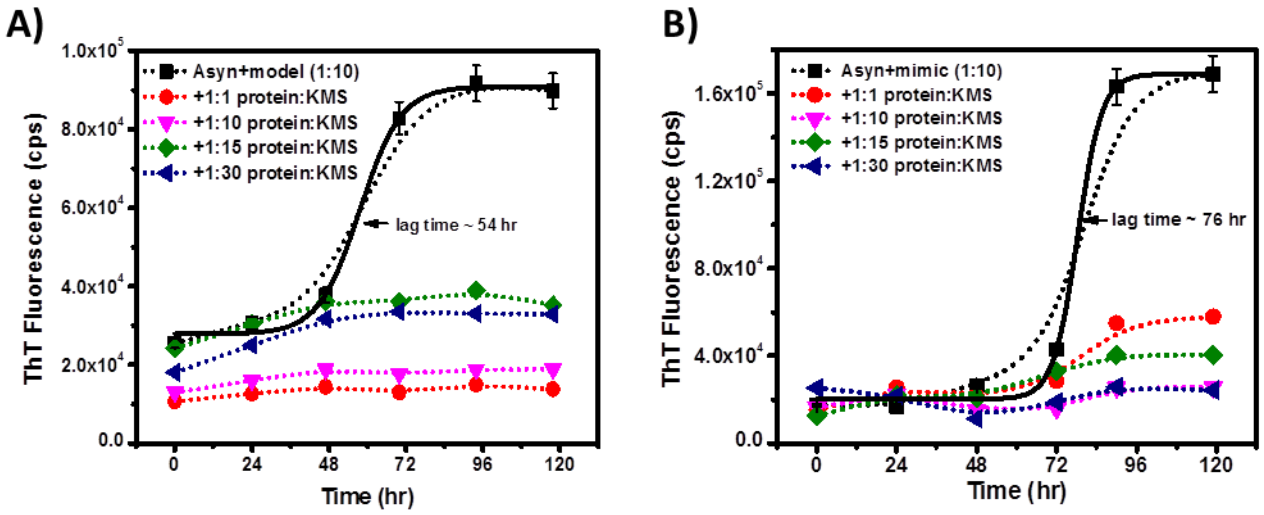

Figure S2. A) ThT-binding assay of A-Syn in presence of model, with and without increasing doses of KMS added. B) ThT-binding assay of A-Syn in presence of mimic, with and without increasing doses of KMS added.

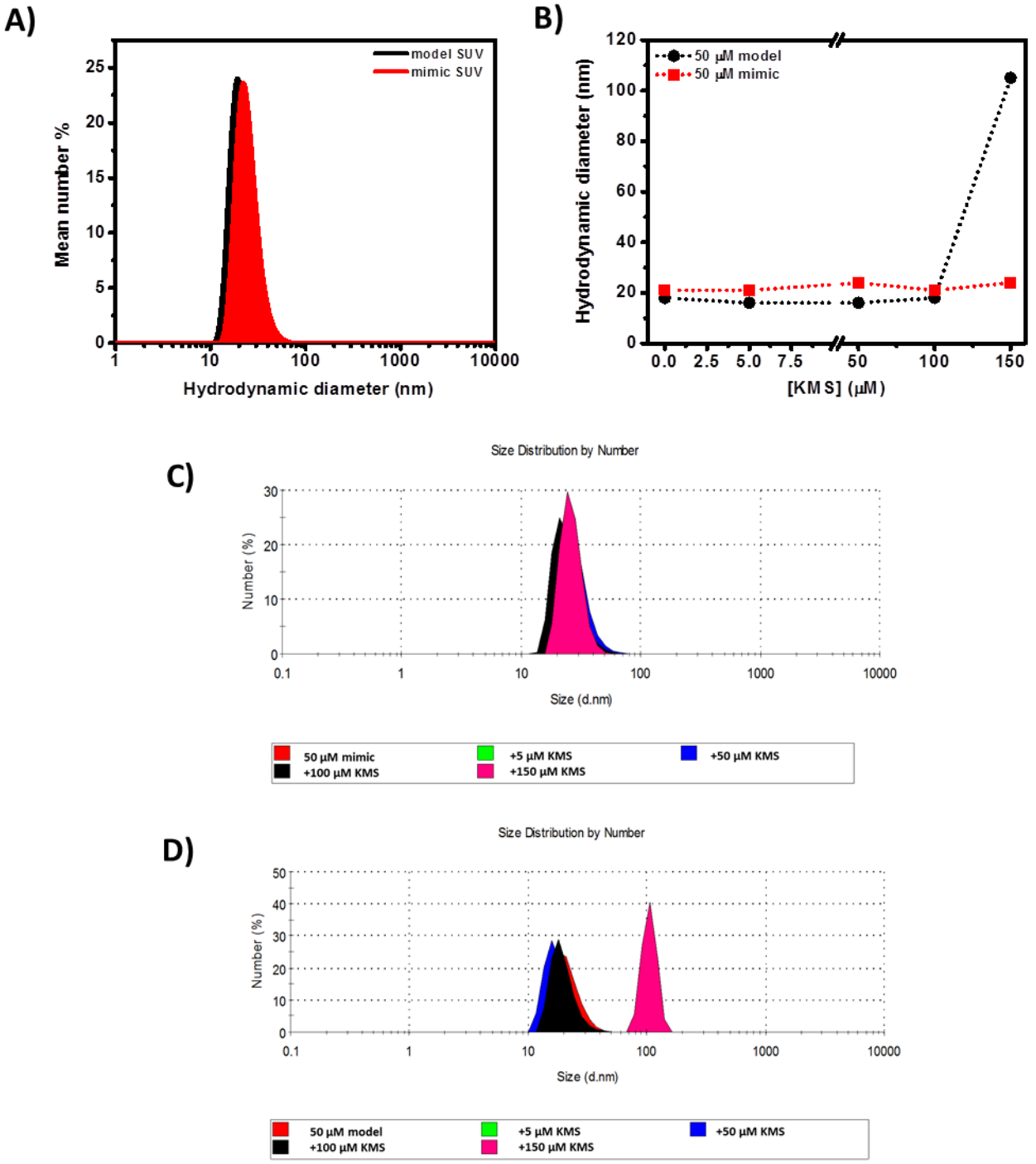

Figure S3. A) Size distribution (by number) of model (black) and mimic (red) SUVs. B) Variation of average hydrodynamic diameter of model (black) and mimic (red) SUVs on addition of increasing amounts of KMS. C) Instrumental graph of size distributions obtained for model with and without increasing amounts of KMS added. D) Instrumental graph of size distributions obtained for mimic with and without increasing amounts of KMS added.

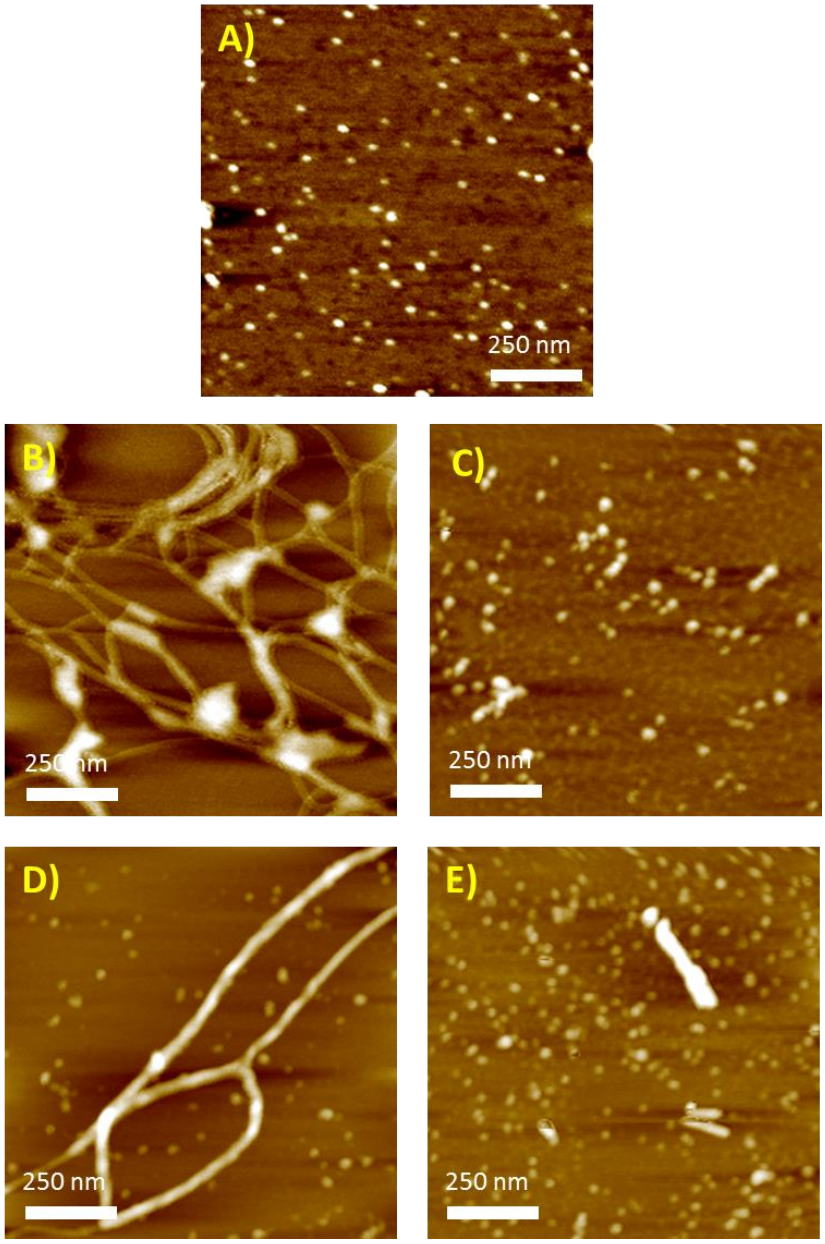

Figure S4. AFM images of A) A-Syn alone after 96 hr of agitation-incubation, showing no fibrils or large aggregates; B) A-Syn after 72 hr of agitation-incubation with model, showing network-like fibrils; C) A-Syn after 72 hr of agitation-incubation with model in presence of KMS, showing broken fibrils and small aggregates; D) A-Syn after 96 hr of agitation-incubation with mimic, showing long and branched fibrils; and E) A-Syn after 96 hr of agitation-incubation with mimic in presence of KMS, showing broken fibrils and small aggregates. Concentrations of protein, lipid and KMS are 5 μM, 50 μM and 50 μM respectively. All AFM images are of dimensions 1.0 μM x 1.0 μM.

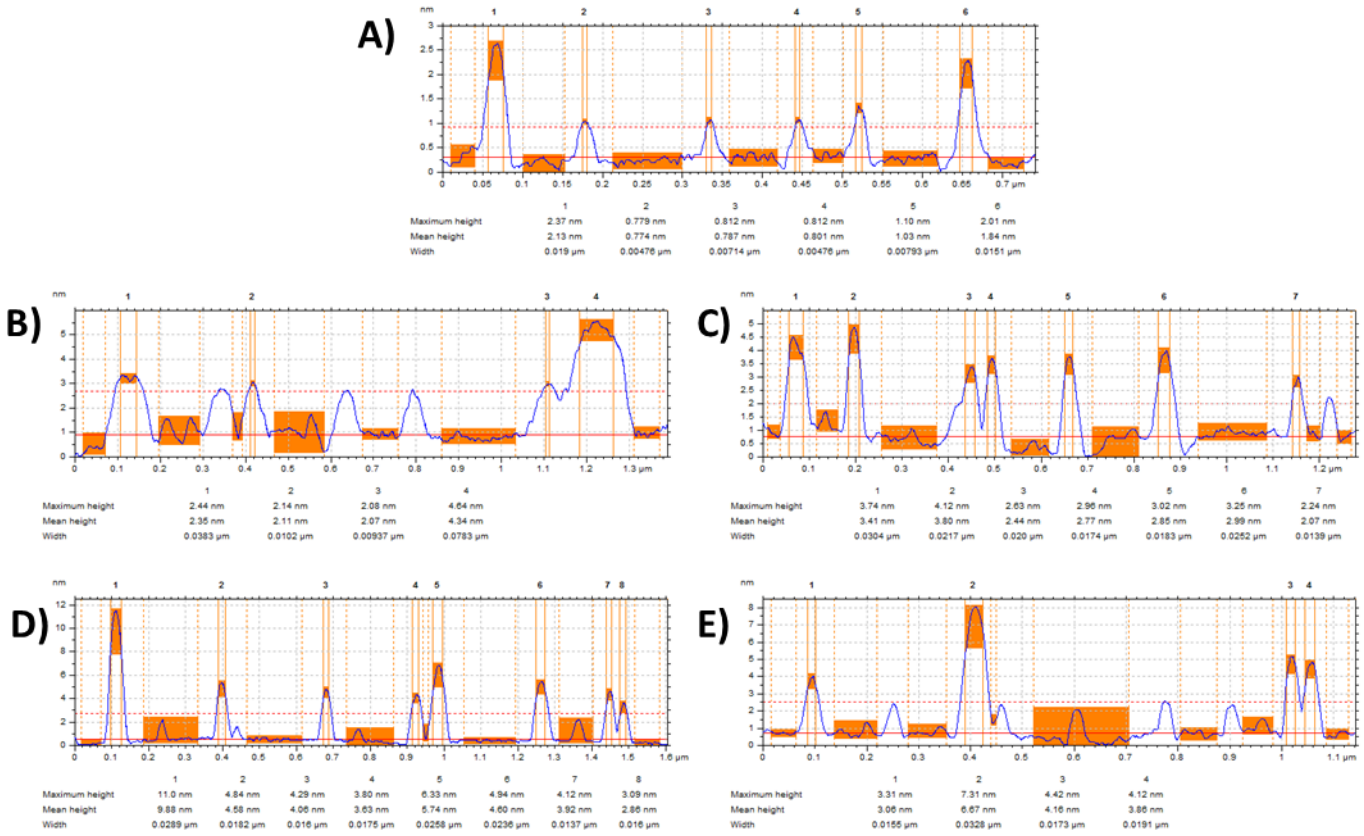

Figure S5. Height distribution profiles from AFM images of samples containing A) 5 µM A-Syn after agitation-incubation for 96 hours, B) 5 µM A-Syn in presence of 10 times model after agitation-incubation for 72 hours, C) 5 µM A-Syn in presence of 10 times model and KMS after agitation-incubation for 72 hours. D) 5 µM A-Syn in presence of 10 times mimic after agitation-incubation for 96 hours and E) 5 µM A-Syn in presence of 10 times mimic and KMS after agitation-incubation for 96 hours.

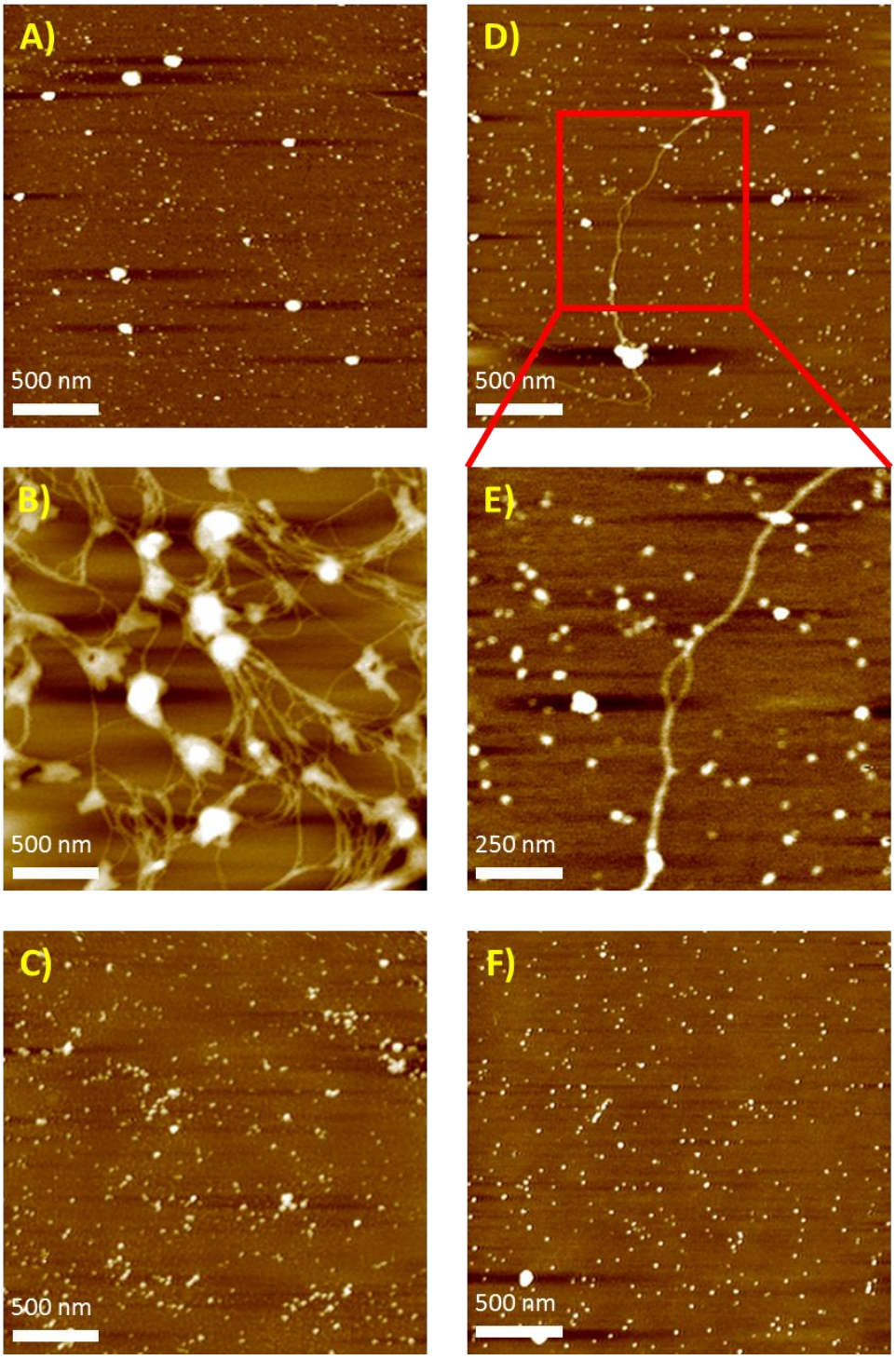

Figure S6. AFM images from another field of samples containing A) 5 µM A-Syn after agitation-incubation for 96 hours, B) 5 µM A-Syn in presence of 10 times model after agitation-incubation for 72 hours, C) 5 µM A-Syn in presence of 10 times model and KMS after agitation-incubation for 72 hours. D) 5 µM A-Syn in presence of 10 times mimic after agitation-incubation for 96 hours, E) Enlarged view of central portion of long fibril in (D) showing branching nature of fibril, and F) 5 µM A-Syn in presence of 10 times mimic and KMS after agitation-incubation for 96 hours. AFM images in A-D and F are 2.5 µM x 2.5 µM in dimension, while E is 1.0 µM x 1.0 µM.

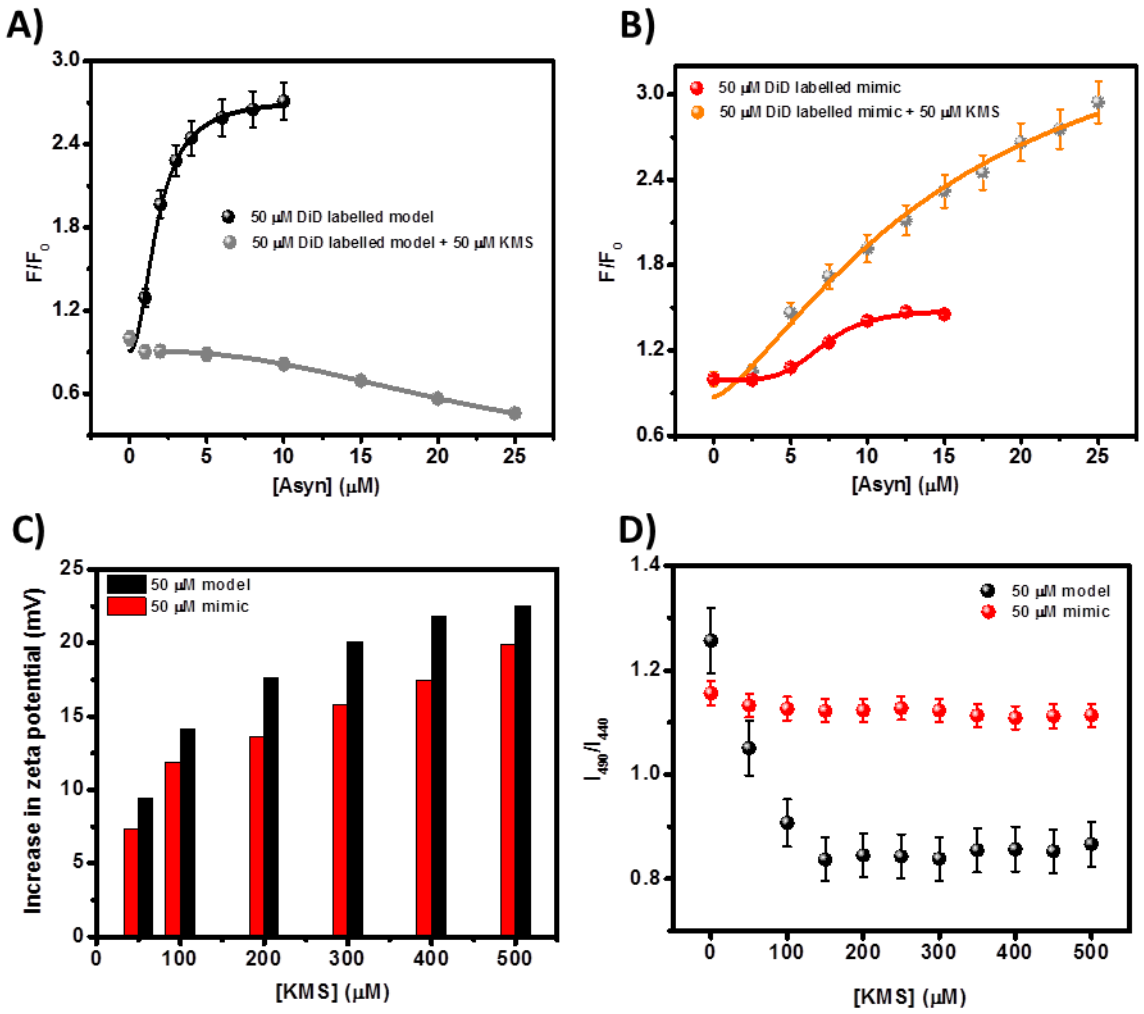

Figure S7. A) Titration curves of A-Syn into model SUVs in the absence (black) and presence (grey) of KMS; B) Titration curves of A-Syn into mimic SUVs in the absence (red) and presence (orange) of KMS. The apparent association constants are tabulated in Table 1 of manuscript. C) The screening effect of KMS on model and mimic membranes, showing higher screening for purely negatively charged model (DOPS) membrane by the positively charged small molecule KMS. D) Effect of KMS on fluidity of model and mimic SUVs, showing how KMS reduced fluidity of the former while latter remains unaffected.

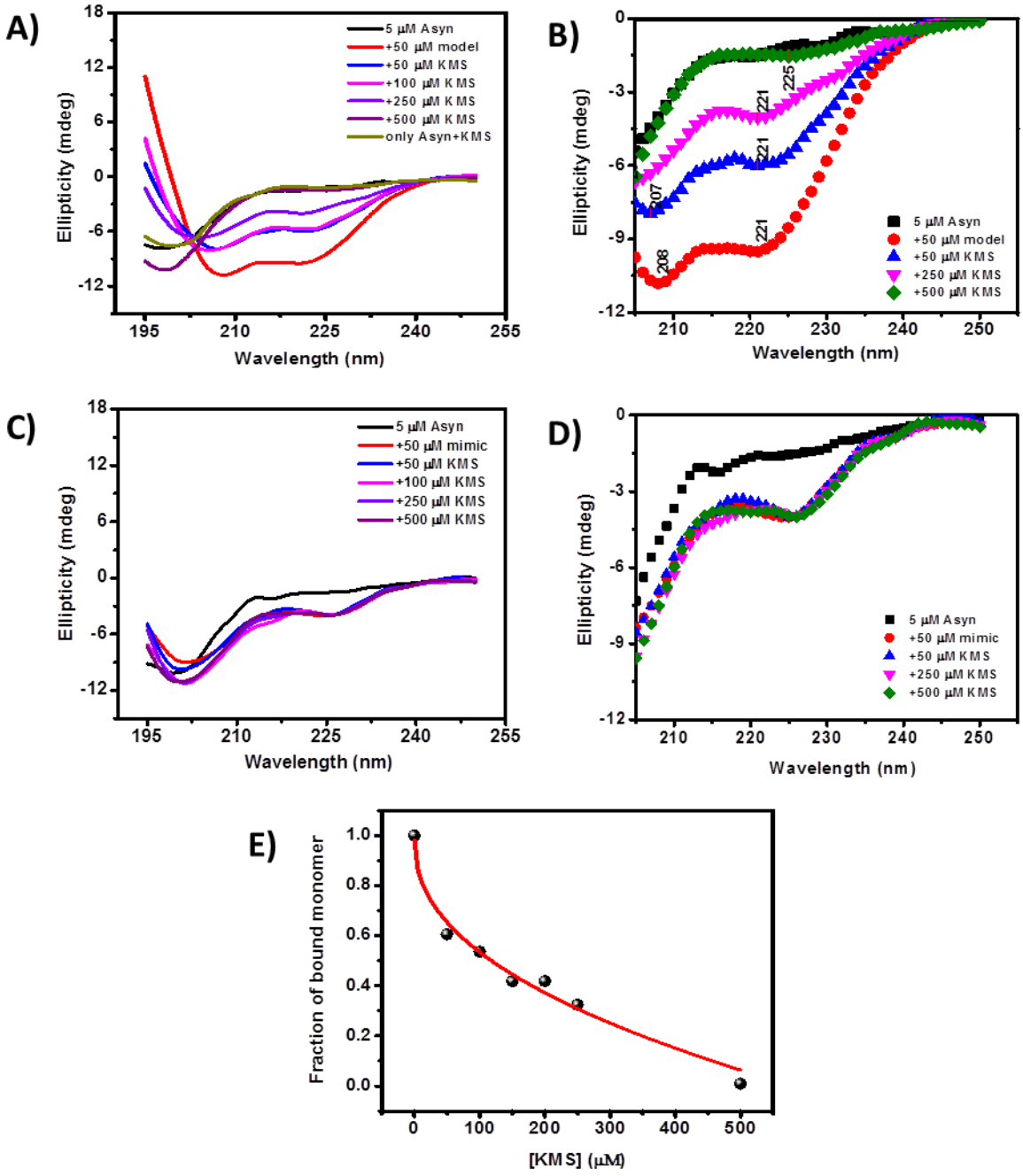

Figure S8. A) CD spectra of A-Syn (black), A-Syn bound to model SUVs (red) and same with increasing concentrations of KMS added. Spectrum of A-Syn with only 500 μM of KMS is also shown for comparison (olive). B) Same as A), but showing partial view of fewer spectra for clarity. C) CD spectra of A-Syn (black), A-Syn bound to mimic SUVs (red) and same with increasing concentrations of KMS added. D) Same as C), but showing partial view of fewer spectra for clarity. E) Plot showing decrease in fraction of model-bound monomer (A-Syn) with increase in concentration of KMS added.

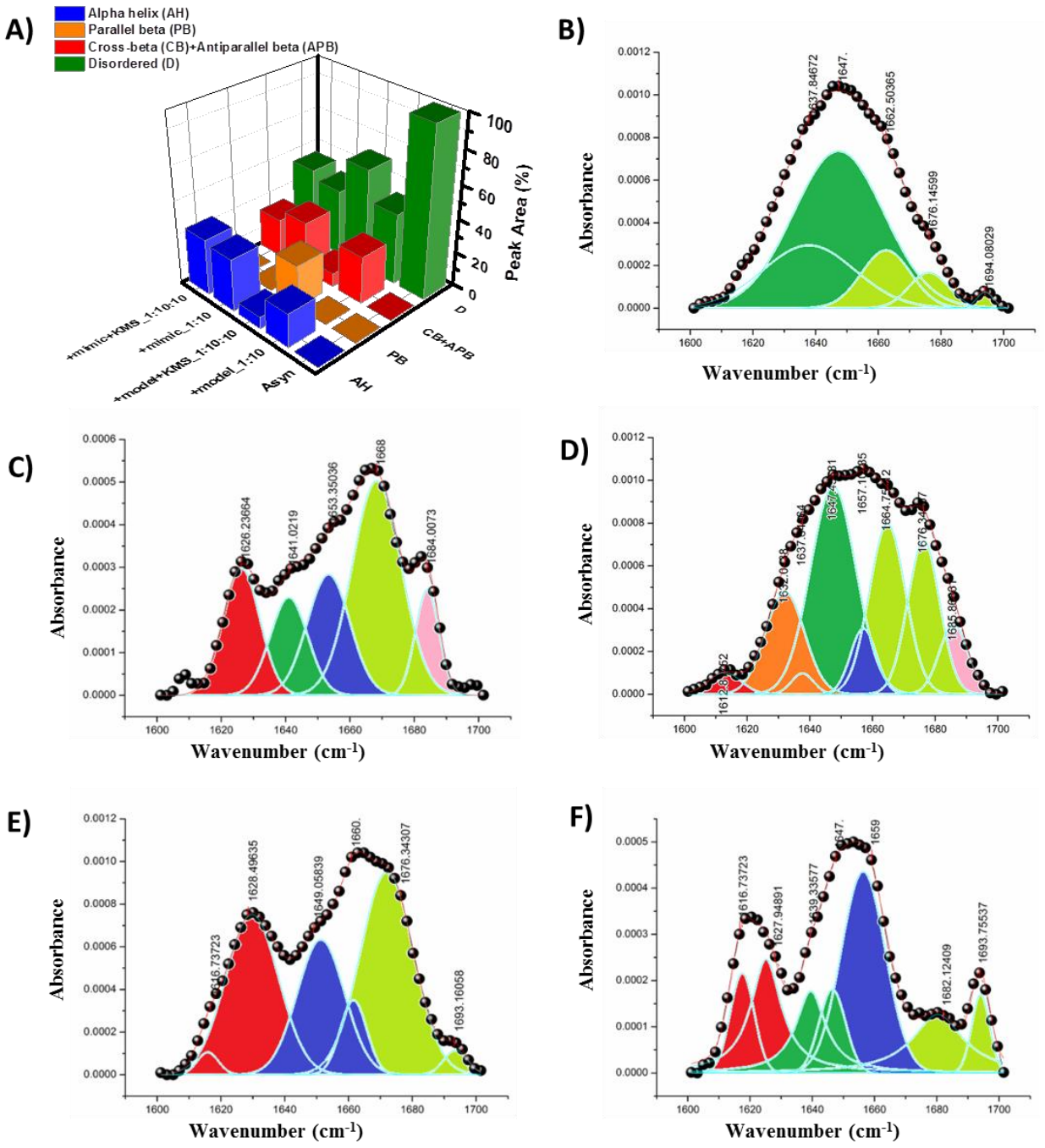

Figure S9. A) 3D bar plot showing relative contents of secondary structure in A-Syn, with and without lipids and inhibitor added. B) to F) Background corrected, baseline-subtracted de-convoluted FTIR spectra of A-Syn, A-Syn with model, A-Syn with model and KMS, A-Syn with mimic, and A-Syn with mimic and KMS, respectively. Red, orange, dark green, blue, light green, and light pink represent cross beta, parallel beta, extended (disorder), alpha helical, loops/turns(disorder) and anti-parallel beta secondary structural contents. Concentrations of protein, lipid and KMS are 100, 1000 and 1000 μM respectively.

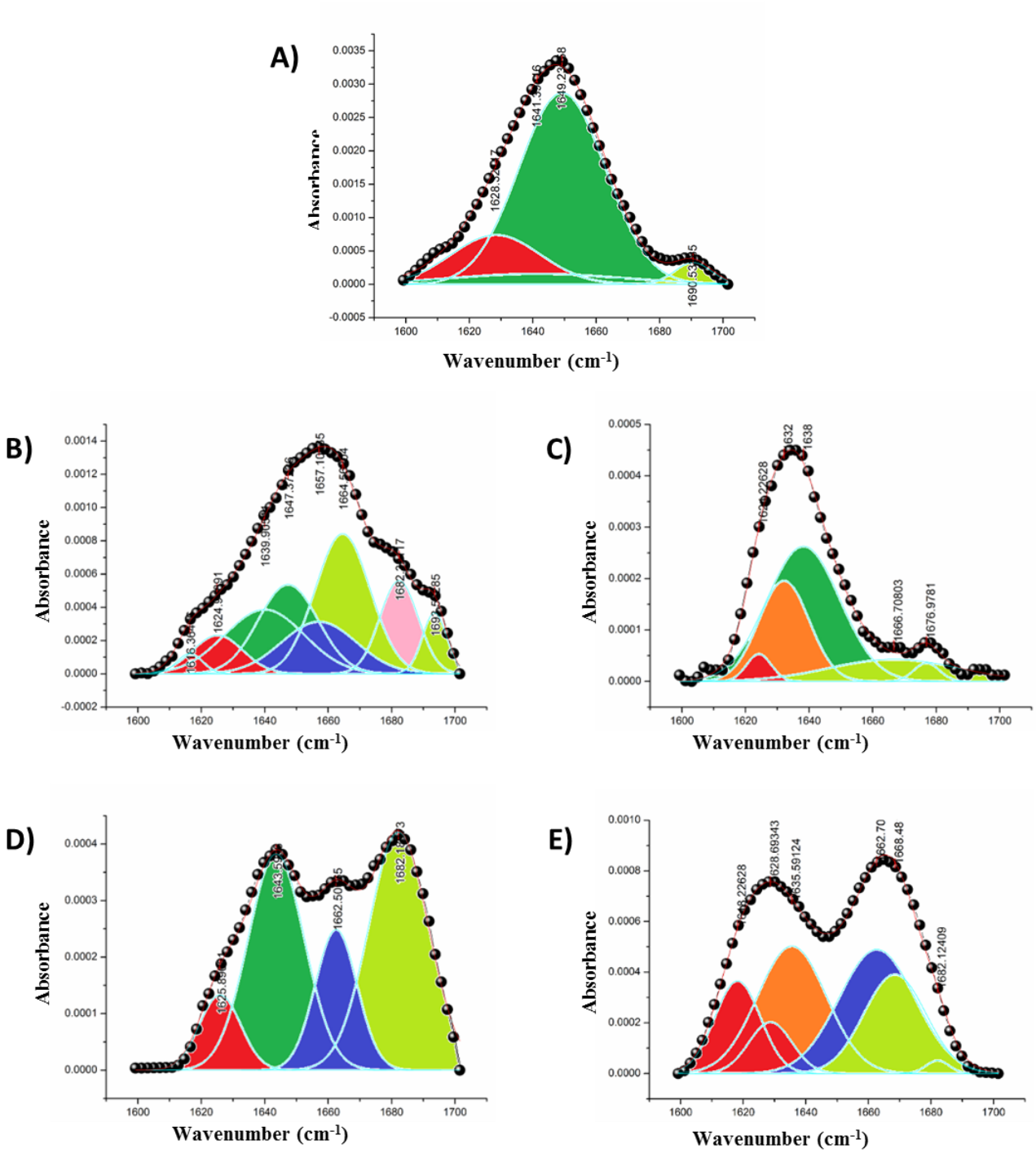

Figure S10. Background corrected, baseline-subtracted de-convoluted FTIR spectra of A) A-Syn, B) A-Syn with model, C) A-Syn with model and KMS, D) A-Syn with mimic, and E) A-Syn with mimic and KMS respectively, after 24 hours of agitation-incubation. Red, orange, dark green, blue, light green, and light pink represent cross beta, parallel beta, extended (disorder), alpha helical, loops/turns(disorder) and anti-parallel beta secondary structural contents. Concentrations of protein, lipid and KMS are 100, 1000 and 1000 μM respectively.

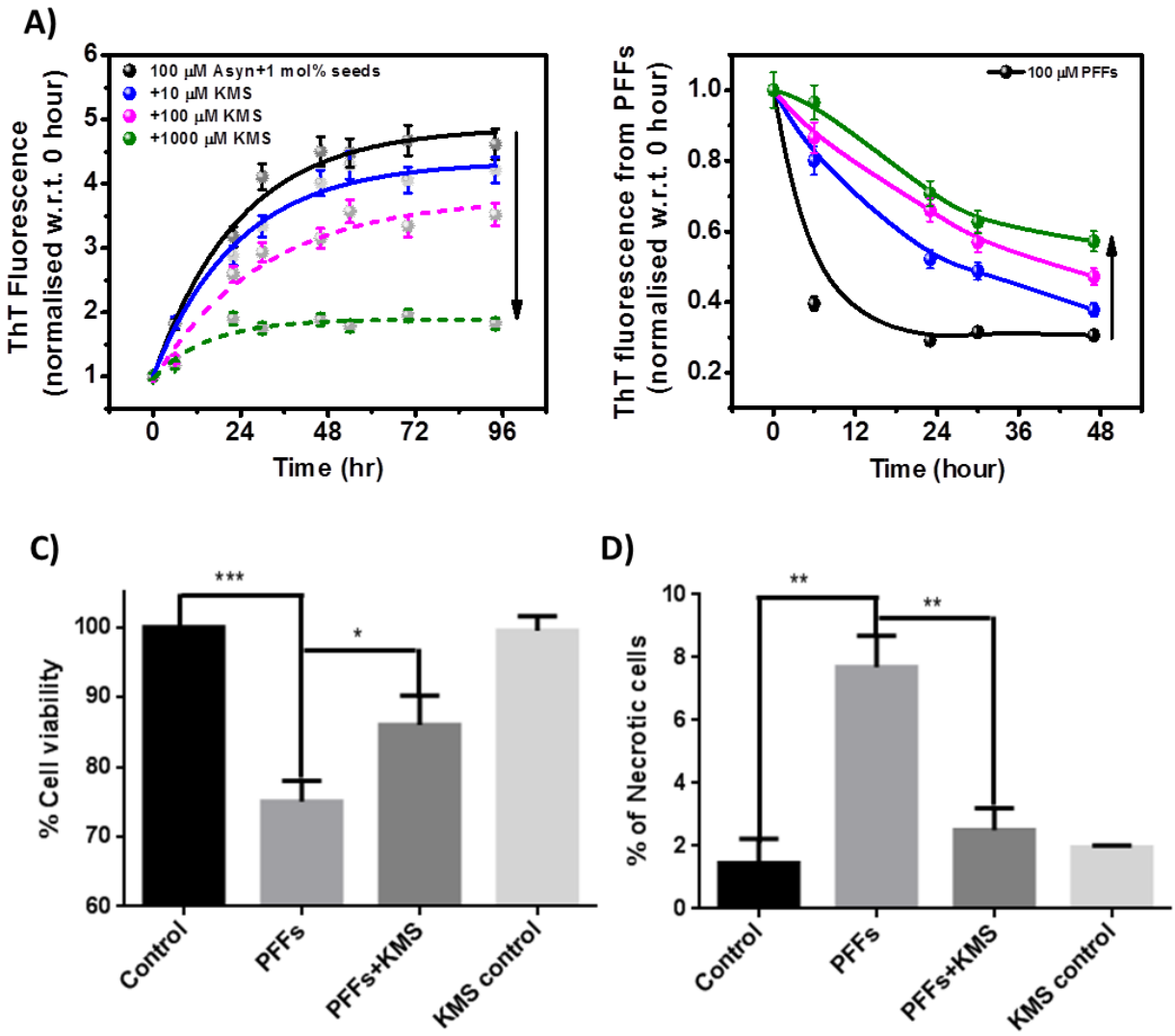

Figure S11. A) ThT assay showing dose-dependent inhibition of seeded secondary nucleation by KMS. The exponential growth rate was almost same with 10 µM KMS, whereas profile for A-Syn with higher concentrations of KMS added could not be fit into any growth profile. B) ThT fluorescence from PFFs in the absence and presence of increasing concentrations of KMS (10, 100 and 1000 µM), over a course of 48 hours under agitation-incubation. KMS concentration increases in the direction of the arrow. C) Cell viability and D) Necrotic cell population of SHSY5Y cells 24 hours after addition of 10 µM of PFFs incubated for 1 hour with and without 10 times KMS. Cell viability in presence of the concentration of KMS used in our studies are also shown, all w.r.t the untreated control. Statistical significances are indicated by *: $p \leq 0.05$, **: $p \leq 0.01$, ***: $p \leq 0.001$, ****: $p \leq 0.0001$.

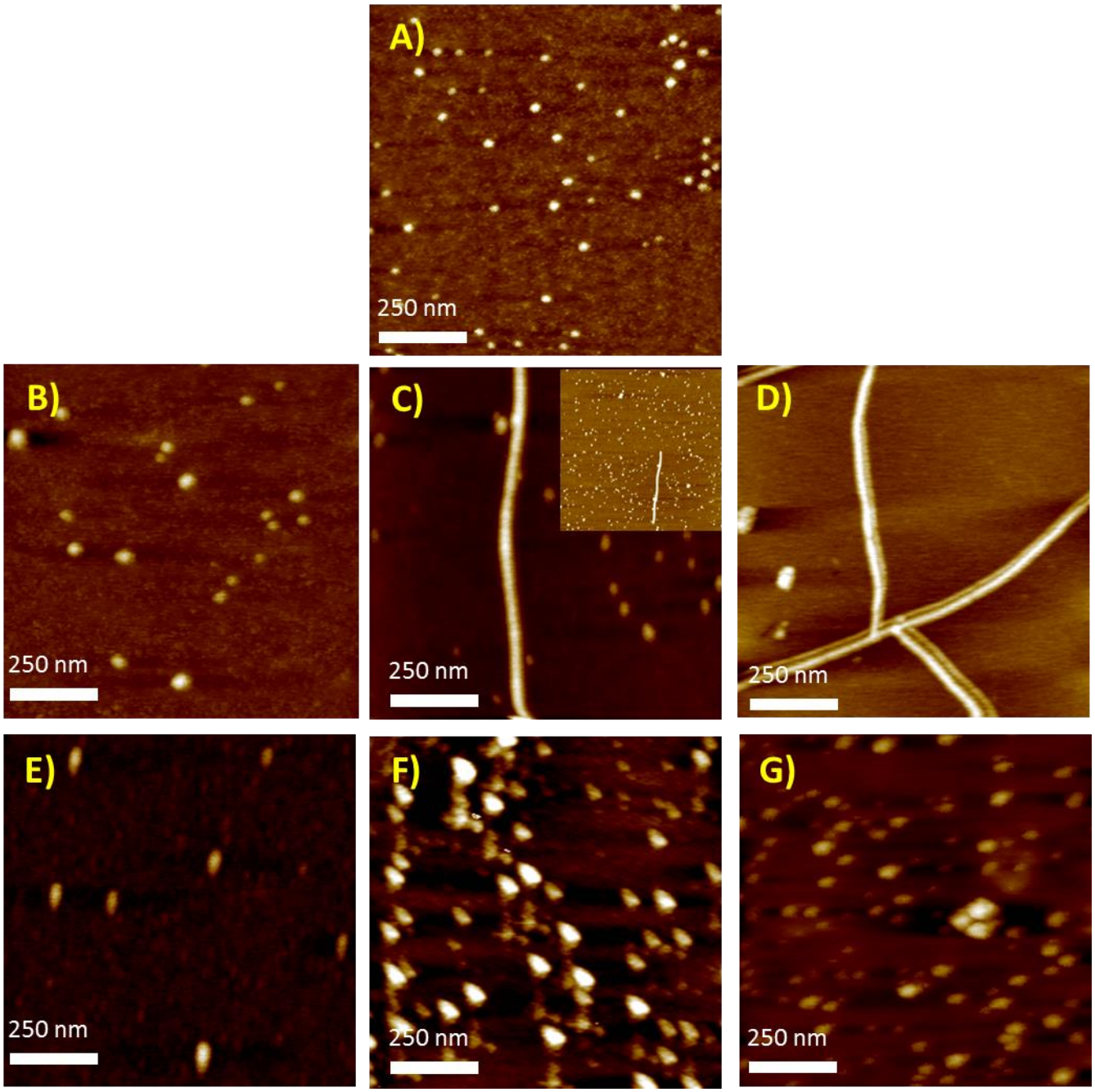

Figure S12. A) to D) are AFM images (1.0 µM x 1.0 µM) of A-Syn samples from 0, 24, 48 and 96 hours of agitation-incubation respectively, showing the transition of monomers (in A) to small oligomers (in B) to proto-fibrils (in C) and ultimately to fibrils (in D). Inset in C) shows a lower magnification view (4.5 µM x 4.5 µM) of the whole proto-fibril. E) to G) show KMS treated A-Syn after 24, 48 and 96 hours of agitation-incubation respectively, showing no formation of fibrils, but formation of amorphous aggregates.

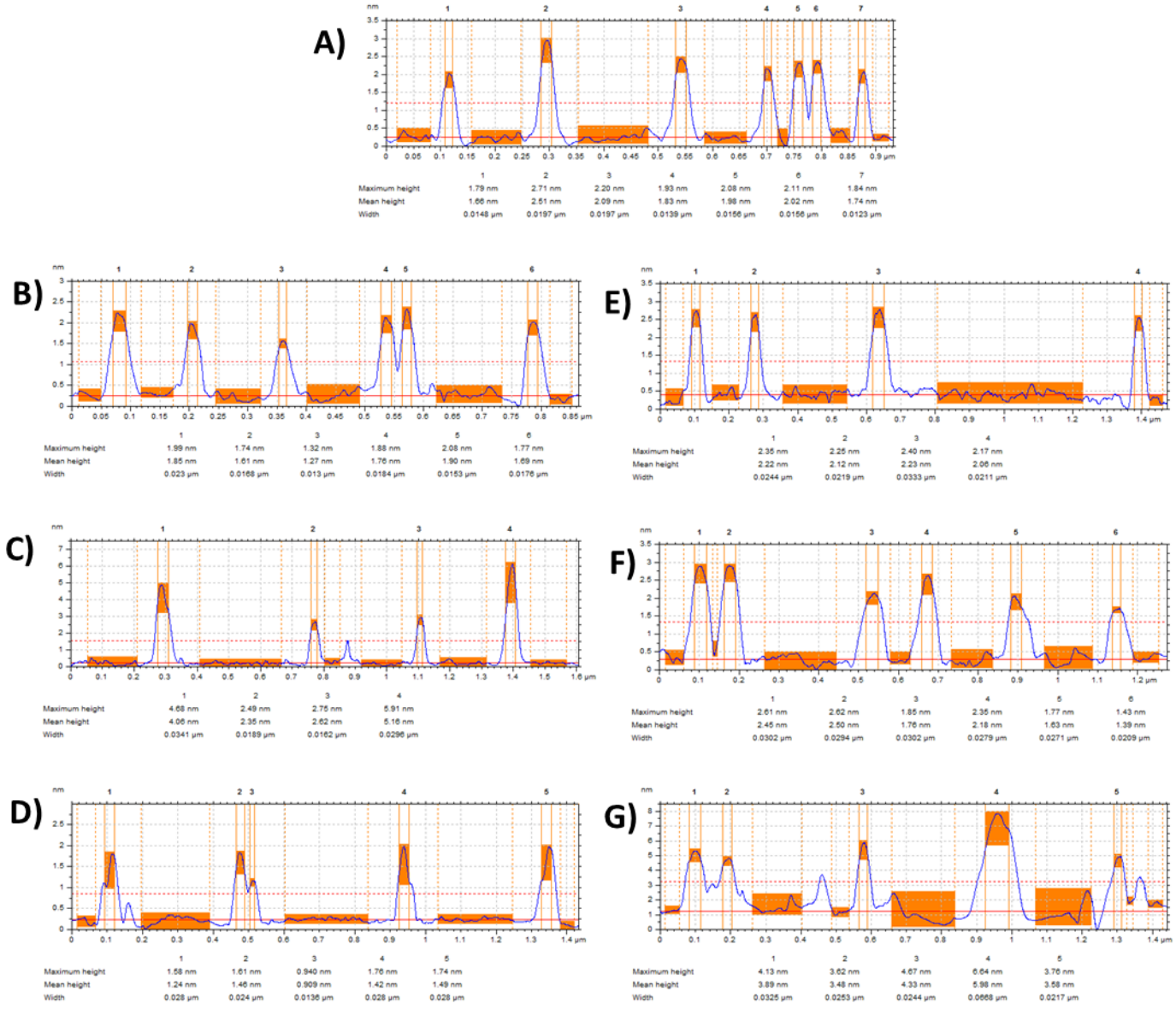

Figure S13. Height distribution profiles from AFM images of samples containing A) native A-Syn, B) A-Syn after 24 hours, C) A-Syn after 48 hours, D) A-Syn after 96 hours, E) KMS treated A-Syn after 24 hours, F) KMS treated A-Syn after 48 hours and G) KMS treated A-Syn after 96 hours of agitation-incubation.

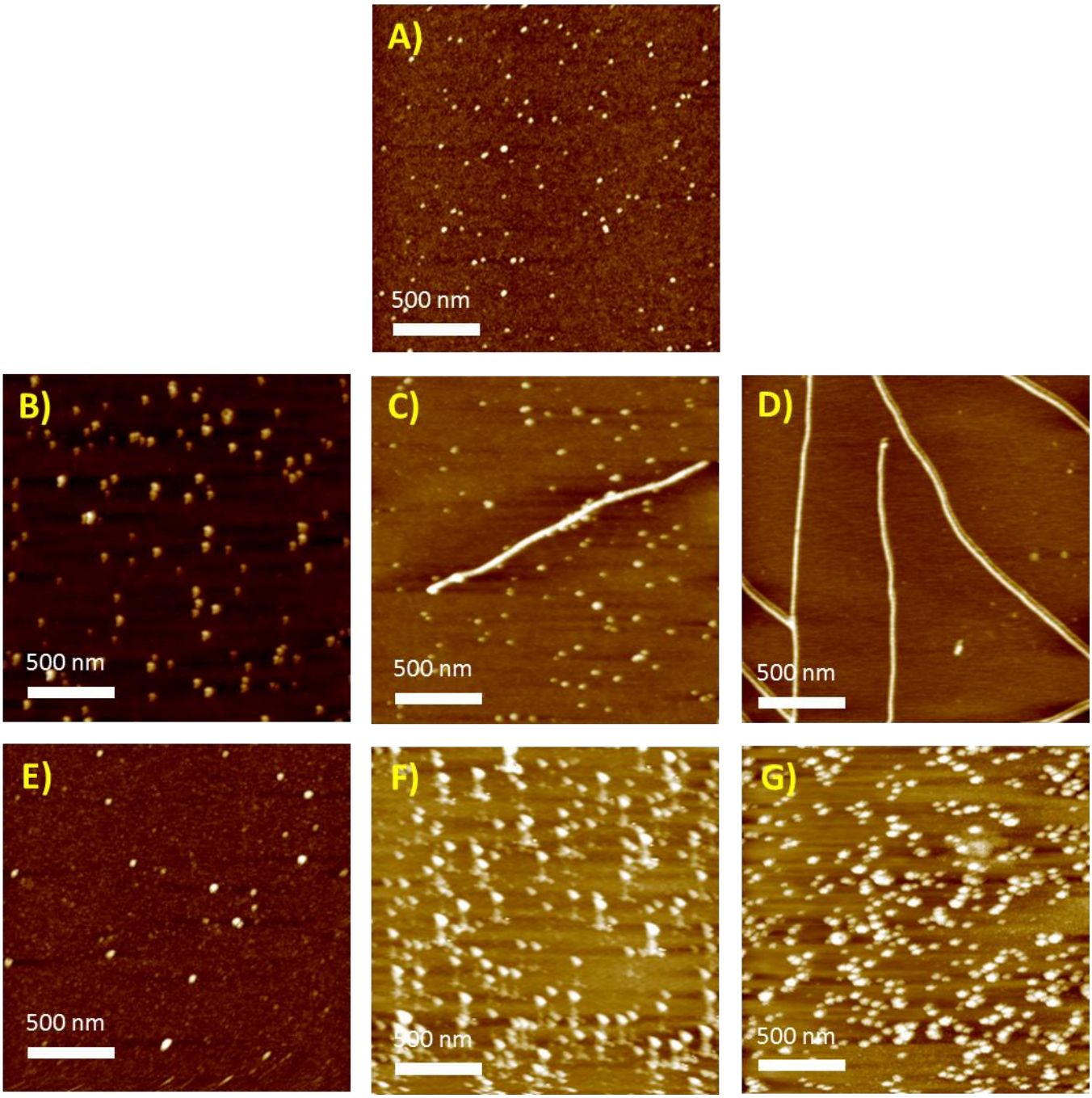

Figure S14. AFM images from another field of samples containing A) native A-Syn, B) A-Syn after 24 hours, C) A-Syn after 48 hours, D) A-Syn after 96 hours, E) KMS treated A-Syn after 24 hours, F) KMS treated A-Syn after 48 hours and G) KMS treated A-Syn after 96 hours of agitation-incubation. AFM images are 2.0 µM x 2.0 µM in dimension.

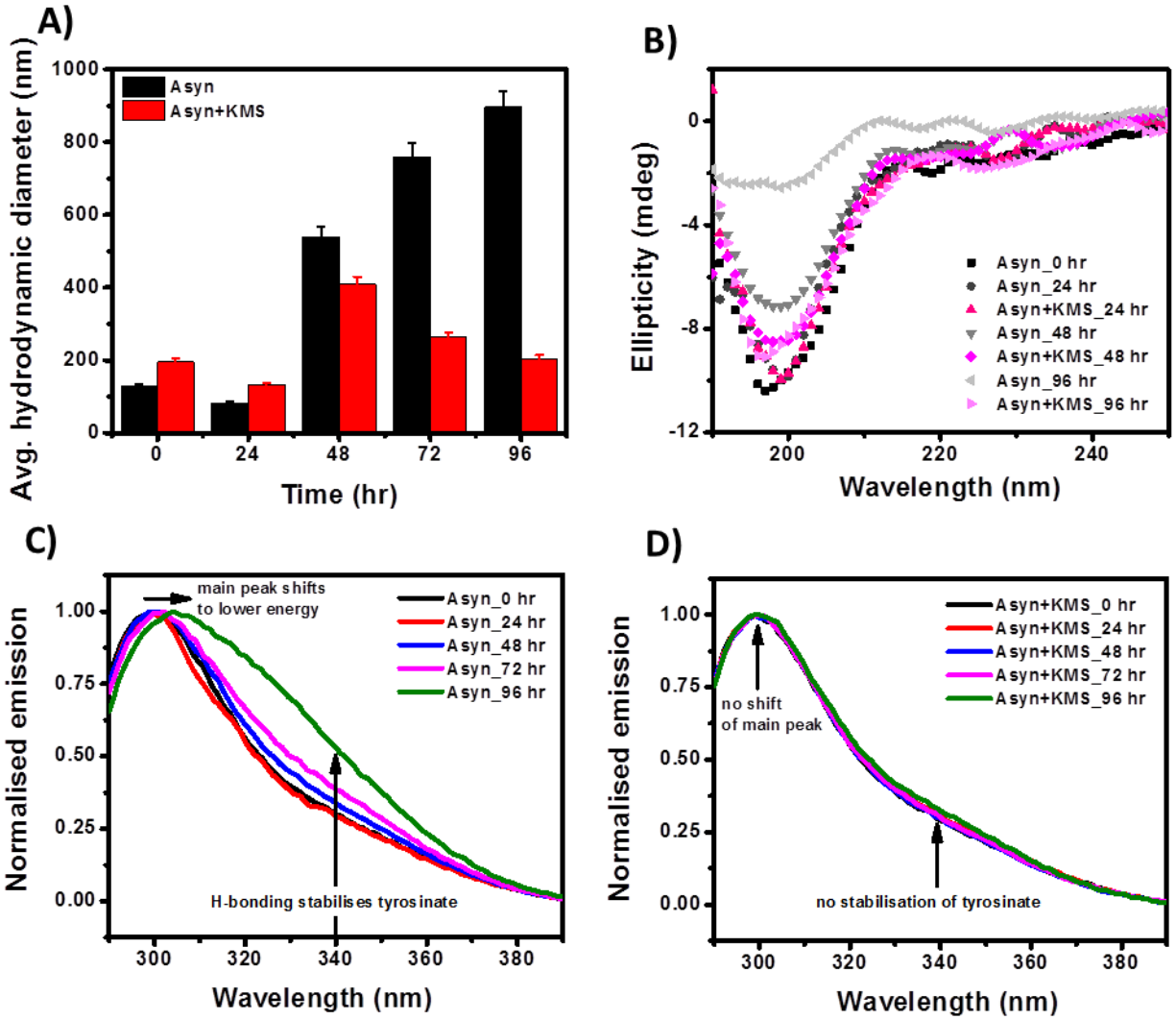

Figure S15. A) Change in particle size of A-Syn (black) and KMS treated A-Syn (red) in course of the aggregation pathway. B) CD spectra of native A-Syn (black trace), along with those of A-Syn and KMS-treated A-Syn recorded after different time-points of agitation-incubation (24, 48 and 96 hours), showing no significant conformational change in case of the latter. C) Normalized tyrosine emission spectra of A-Syn at different time points of aggregation showing increase in tyrosinate intensity (~340 nm). D) Normalized tyrosine emission spectra of KMS-treated A-Syn at different time points of aggregation showing no noticeable increase in tyrosinate intensity.

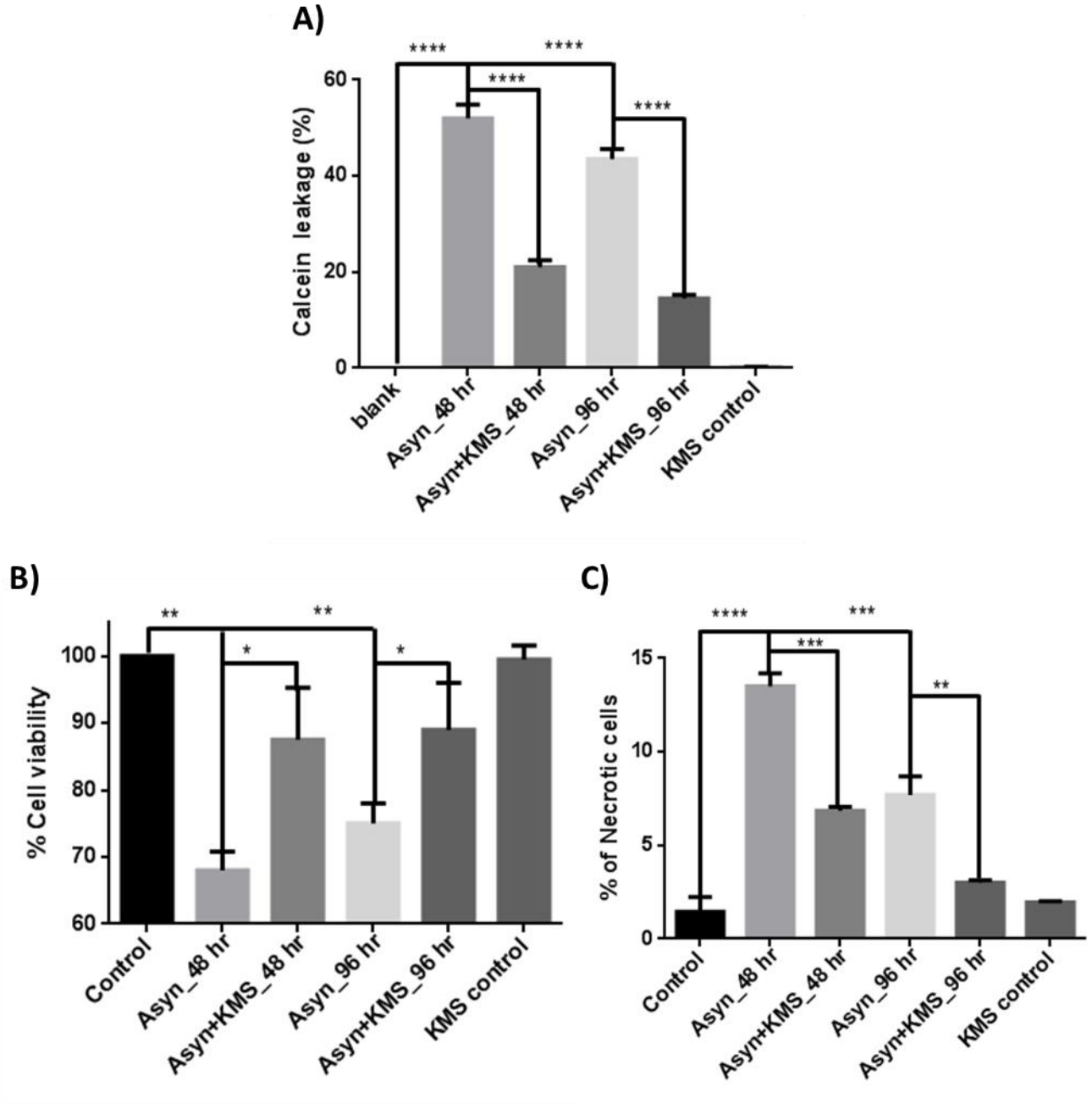

Figure S16. A) Changes in liposomal membrane permeability upon the addition of A-Syn and KMS-treated A-Syn aggregated for 48 and 96 hours, showing stabilizing effect on membranes by KMS-modified aggregates w.r.t. only A-Syn counterparts. B) Cell viability and C) Necrotic cell population of SHSY5Y cells 24 hours after addition of 10 μM of A-Syn pre-incubated for 48 and 96 hours in the absence and presence of KMS. Cell viability in presence of the concentration of KMS used in our studies are also shown, all w.r.t the untreated control. Protein:KMS ratio is 1:10 in all three studies. Statistical significances are indicated by *: $p \leq 0.05$, **: $p \leq 0.01$, ***: $p \leq 0.001$, ****: $p \leq 0.0001$.

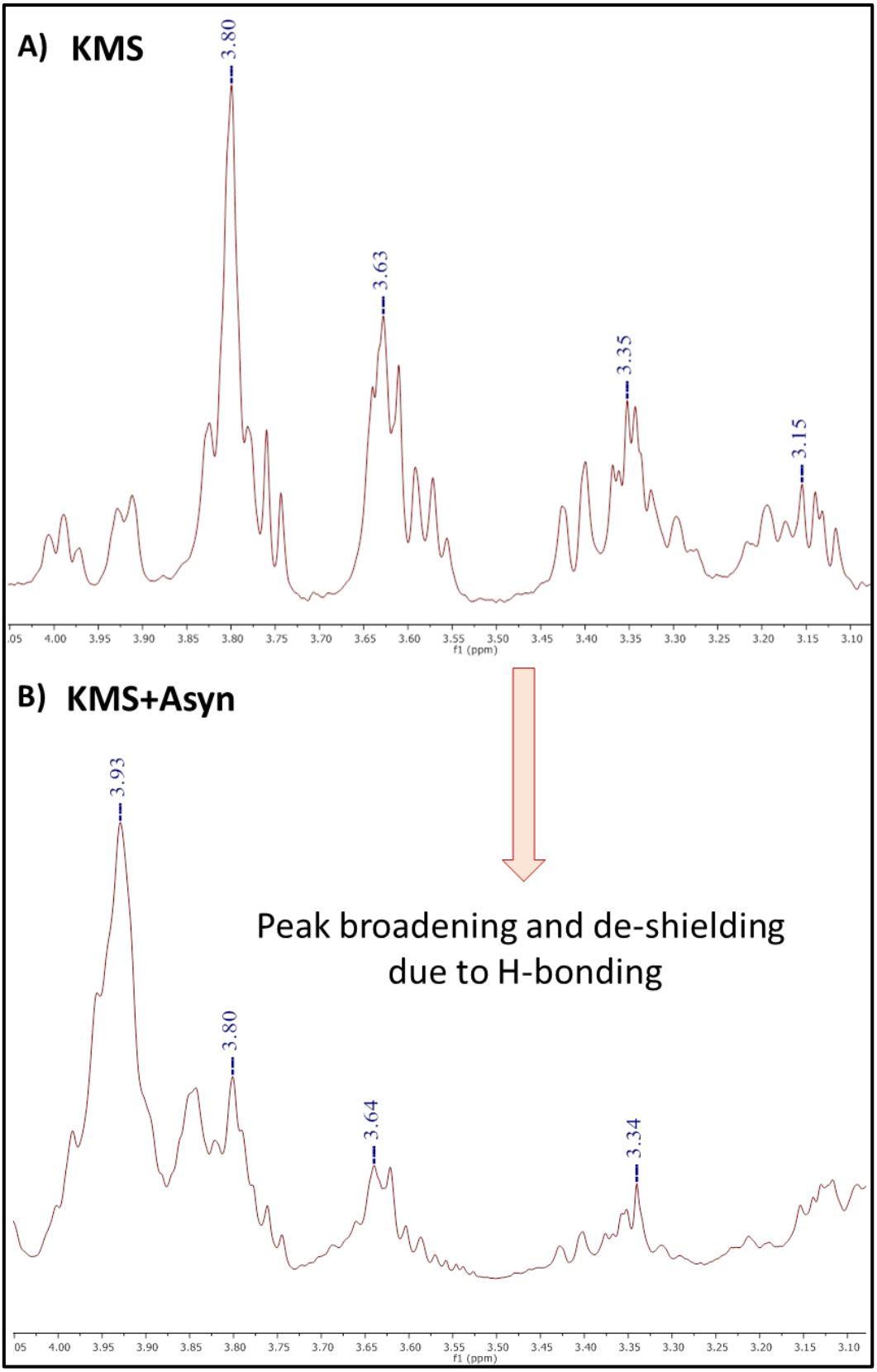

Figure S17. Zoomed in ^{1}H NMR spectra of A) KMS, and B) KMS mixed with A-Syn, between 3.0 and 4.0 δ_{ppm}, showing the shift (and broadening) of peaks corresponding to the H-bond donors towards higher δ_{ppm}values.

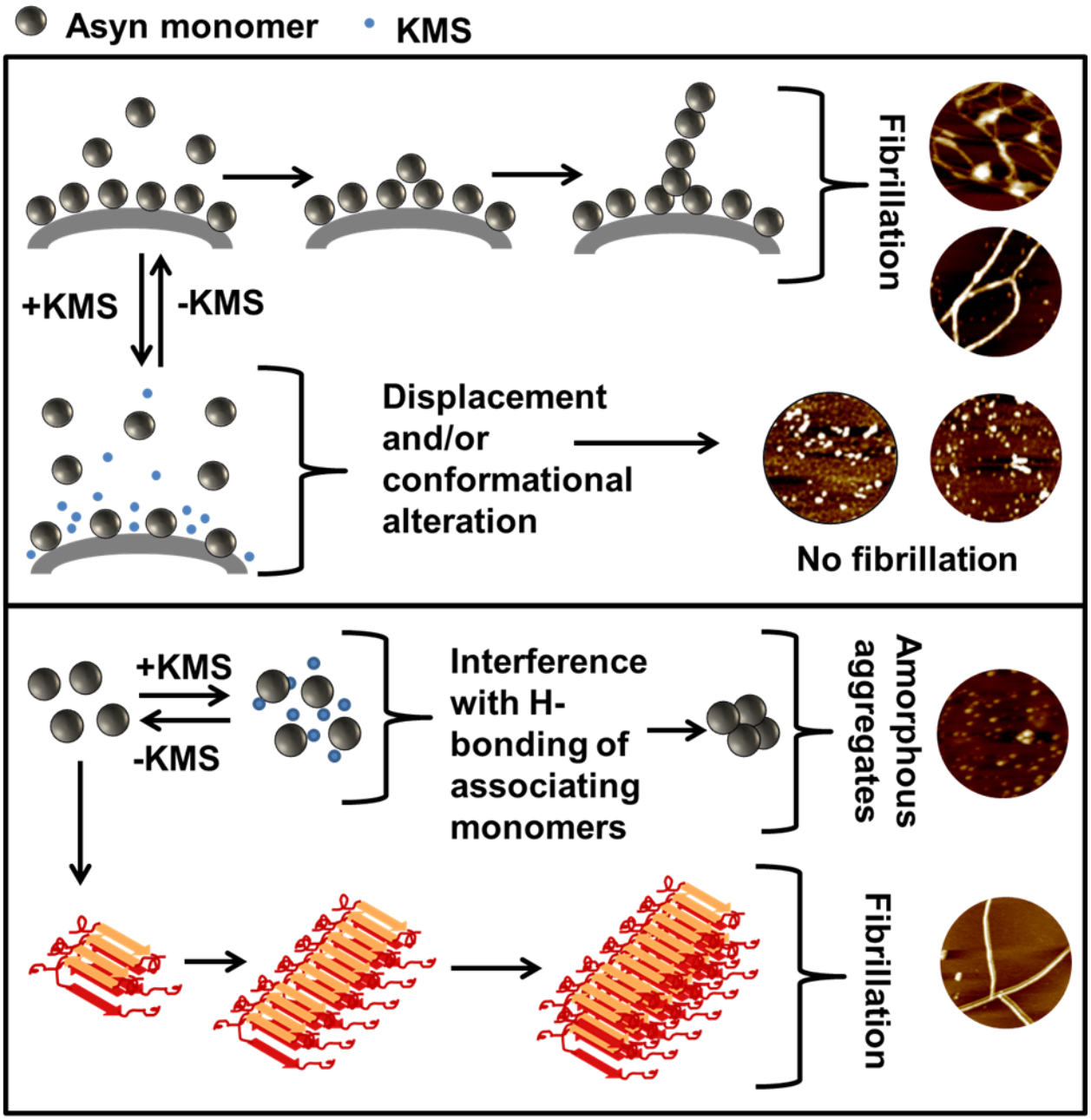

Figure S18. Schematic representation of how Kanamycin interferes with the lipid-induced (top) and solution-phase (bottom) fibrillation of A-Syn.

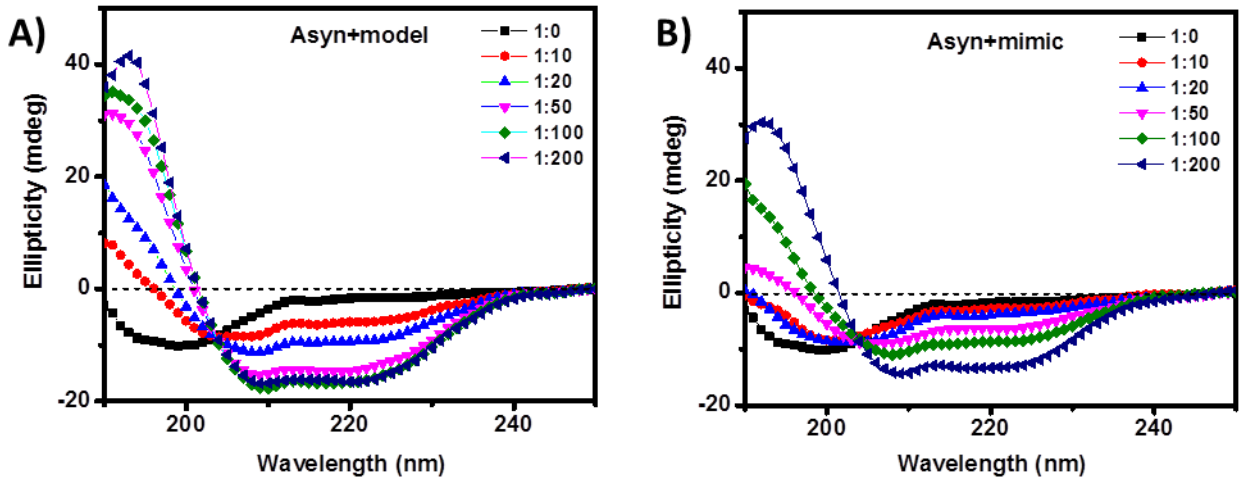

Figure S19. CD spectra showing the acquisition of helical structure by A-Synon binding to A) model and B) mimic SUVs.Protein:lipid ratios are mentioned in the inset.

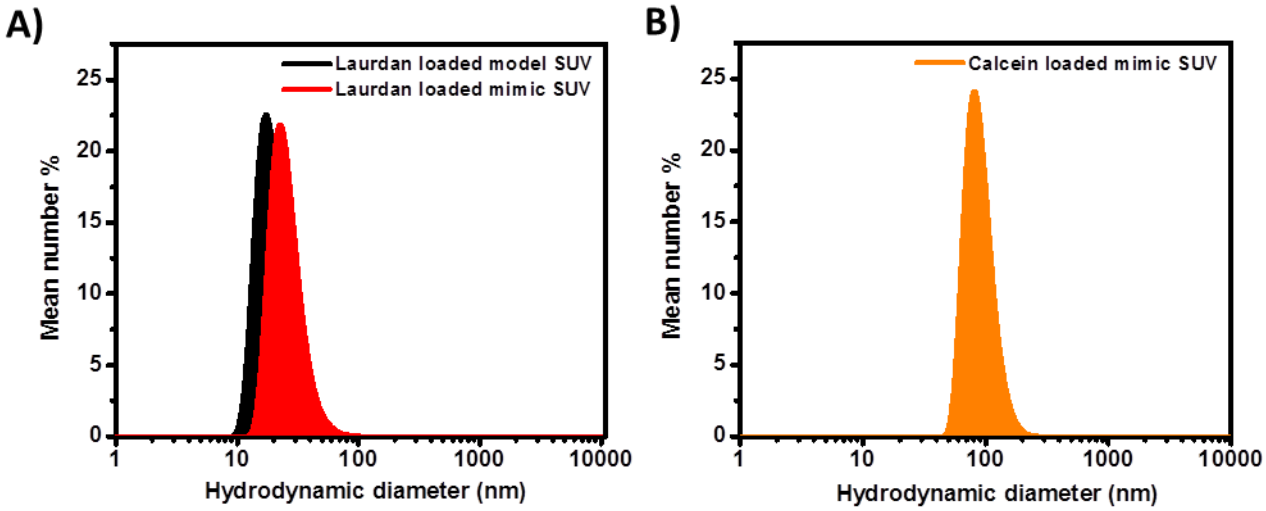

Figure S20. Size distribution of A) Laurdan-loaded model (black) and mimic (red) SUVs; B) Calcein loaded mimic SUVs.

Table S1. Percentages of secondary structure obtained from analysis of FTIR data.

		Cross beta (1611−1630 cm−1)	**Parallel beta(1630-1637 cm-1)**	**Disordered /Extended (1637-1649 cm-1)**	**Alpha helix (1649−1662 cm−1)**	**Disordered/Loops and turns (1662-1682 & 1690-1695 cm-1)**	**Anti-parallel beta (1682-1689 cm-1)**
	Time (hr)						
A-Syn	**0**			80		20	
	24	18		79		3	
A-Syn + model	**0**	18		13	20	39	10
	24	9		35	13	31	12
A-Syn + model + KMS	**0**	2	**15**	32	7	38	6
	24	4	**27**	53		16	4
A-Syn + mimic	**0**	30			31	39	
	24	11		34	17	38	11
A-Syn + mimic + KMS	**0**	23		8	33	36	
	24	21	**28**		30	20	1

3. REFERENCES

(1) Polinski, N. K.; Volpicelli-Daley, L. A.; Sortwell, C. E.; Luk, K. C.; Cremades, N.; Gottler, L. M.; Froula, J.; Duffy, M. F.; Lee, V. M.; Martinez, T. N. *Journal of Parkinson's disease* **2018**, *8*, 303-322.

(2) Bodner, C. R.; Dobson, C. M.; Bax, A. *Journal of molecular biology* **2009**, *390*, 775-790.

(3) Lorenzen, N.; Lemminger, L.; Pedersen, J. N.; Nielsen, S. B.; Otzen, D. E. *FEBS letters* **2014**, *588*, 497-502.

(4) Sannigrahi, A.; Maity, P.; Karmakar, S.; Chattopadhyay, K. *The Journal of Physical Chemistry B* **2017**, *121*, 1824-1834.

(5) Nogues, I. F. T.; Goutayer, M.; Da Silva, A.; Guyon, L.; Djaker, N.; Josserand, V.; Neumann, E.; Bibette, J.; Vinet, F. *Journal of biomedical optics* **2009**, *14*, 054005.

(6) Parasassi, T.; De Stasio, G.; d'Ubaldo, A.; Gratton, E. *Biophysical journal* **1990**, *57*, 1179-1186.

(7) Parasassi, T.; Di Stefano, M.; Loiero, M.; Ravagnan, G.; Gratton, E. *Biophysical Journal* **1994**, *66*, 120-132.

(8) Galvagnion, C. *Journal of Parkinson's disease* **2017**, *7*, 433-450.

(9) Micsonai, A.; Wien, F.; Kernya, L.; Lee, Y.-H.; Goto, Y.; Réfrégiers, M.; Kardos, J. *Proceedings of the National Academy of Sciences* **2015**, *112*, E3095-E3103.

(10) Kong, J.; Yu, S. *Acta biochimica et biophysica Sinica* **2007**, *39*, 549-559.

(11) Sarkar-Banerjee, S.; Chowdhury, S.; Paul, S. S.; Dutta, D.; Ghosh, A.; Chattopadhyay, K. *Biochemistry* **2016**, *55*, 4457-4468.

(12) Goormaghtigh, E.; Cabiaux, V.; RUYSSCHAERT, J. M. *The FEBS Journal* **1990**, *193*, 409-420.

(13) Roeters, S. J.; Iyer, A.; Pletikapić, G.; Kogan, V.; Subramaniam, V.; Woutersen, S. *Scientific reports* **2017**, *7*, 41051.

(14) Cascella, R.; Conti, S.; Tatini, F.; Evangelisti, E.; Scartabelli, T.; Casamenti, F.; Wilson, M. R.; Chiti, F.; Cecchi, C. *Biochimica et Biophysica Acta (BBA)-Molecular Basis of Disease* **2013**, *1832*, 1217-1226.

(15) Venderova, K.; Park, D. S. *Cold Spring Harbor perspectives in medicine* **2012**, *2*, a009365.

(16) Cookson, M. R. *Molecular neurodegeneration* **2009**, *4*, 9.